ELSEVIER

Contents lists available at ScienceDirect

# Deep-Sea Research Part II

journal homepage: http://www.elsevier.com/locate/dsr2





# Ocean currents and gradients of surface layer properties in the vicinity of the Madagascar Ridge (including seamounts) in the South West Indian Ocean

Patrick Vianello <sup>a</sup>, Jean-François Ternon <sup>b,e</sup>, Hervé Demarcq <sup>b,e</sup>, Steven Herbette <sup>c</sup>, Michael J. Roberts <sup>a,d,\*</sup>

- <sup>a</sup> UK-SA NRF/DST Bilateral Research Chair: Ocean Sciences and Marine Food Security, Nelson Mandela University, Port Elizabeth, South Africa
- <sup>b</sup> MARBEC, Univ. Montpellier, CNRS, Ifremer, IRD, Sète, France
- Laboratoire d'Océanographie Physique et Spatiale (LOPS), IUEM, Univ. Brest CNRS IRD Ifremer, Brest, France
- <sup>d</sup> National Oceanography Centre, Southampton, United Kingdom
- <sup>e</sup> Institut de Recherche pour le Développement (IRD), Marseille, France

#### ARTICLE INFO

# Keywords: South West Indian Ocean Madagascar Ridge Seamounts Walters shoal Sea surface temperature Eddy kinetic energy Mixed layer depth Chlorophyll-a Geostrophic currents

## ABSTRACT

This work is part of the MADRidge Project special issue which aims to describe pelagic ecosystems in the vicinity of three prominent shallow seamounts in the South West Indian Ocean: one here named MAD-Ridge (240 m below the surface) plus Walters Shoal (18 m) on the Madagascar Ridge, and La Pérouse (60 m) on the abyssal plain east of Madagascar. The three span latitudes  $20^{\circ}$ S and  $33^{\circ}$ S, some 1500 km. The study provides the background oceanography for the once-off, multidisciplinary snapshot cruise studies around the seamounts. As life on seamounts is determined by factors such as summit depth, proximity to the light layers of the ocean, and the ambient circulation, a first description of regional spatial-field climatologies (16–22 years) and monthly along-ridge gradients of surface wind (driving force), water column properties of sea surface temperature, mixed layer depth, chlorophyll- $\alpha$  and eddy kinetic energy, plus ocean currents is provided. Being relevant to many applications in the study domain, these properties in particular reveal contrasting environments along the Madagascar Ridge and between the three seamounts that should drive biological differences. Relative to the other two seamounts, MAD-Ridge is in the more extreme situation, being at the end of the East Madagascar Current, where it experiences sturdy, albeit variable, currents and the frequent passing of mesoscale eddies.

# 1. Introduction

# 1.1. Importance of ridges and seamounts

Most of the world's extensive seafloor consists of a deep muddy plain inhabited by molluscs, worms and echinoderms (Thistle, 2003). Bathypelagic fish are few. It is only sharp ridges and seamounts that provide a deep-sea relief, rocky and sediment-free, that can support abundant diverse and distinctive fauna. Seamounts are of volcanic origin, and tend to be on the oceanic crust near mid-ocean ridges, mantle plumes (hotspots) and island arcs (Keating et al., 1987). They range from isolated landmarks to clusters and chains (Roberts et al., 2020). Estimates of the number of seamounts in the global ocean vary between 10 000 and 100

000 (Kitchingman et al., 2007; Harris et al., 2014). The total area of these features is equivalent to about 30% of the global shelf region, making them significant platforms in sustaining life in the vast, deep ocean. With structure for animals to settle and live on, and currents supplying nutrients and food, the variety of life at seamounts is often great. This situation has been noticed by fishers who, in many cases, have plundered species of commercial value such as the deep-living orange roughy (Hoplostethus atlanticus) and Patagonian toothfish (Dissostichus eleginoides) at the base of seamounts, and various tuna species and swordfish around the summits.

However, given the large number of seamounts globally and their remote locations, much about the structure, function and connectivity of seamount ecosystems remains unexplored and unknown. Threats such

E-mail address: mike.roberts@mandela.ac.za (M.J. Roberts).

<sup>\*</sup> Corresponding author. UK-SA NRF/DST Bilateral Research Chair: Ocean Sciences and Marine Food Security, Nelson Mandela University, Port Elizabeth, South Africa.

as fishing and seabed mining are creating an unprecedented demand for research to inform conservation and management strategies. Clark et al. (2012) in particular called for renewed and intensive scientific effort to enhance the physical and biological information on seamount location, physical characteristics, comprehensiveness of biodiversity inventories, and the understanding of seamount connectivity and faunal dispersal.

## 1.2. What shapes life on seamounts?

Most seamounts lie deep beneath the ocean surface, rising <1500 m from the abyssal plains. A few reach the photic zone, and even fewer protrude above the ocean surface to form islands. Their volcanic nature and steep sides mean that bottom sediment loads tend to be low, providing islands of exposed hard substratum in the wider ocean. However, there are also other factors that determine the nature of the benthic and pelagic ecosystems that evolve around seamounts. Shape and summit depth determine the interactions with the surrounding oceanography, especially currents. Current velocities are strongest at the surface but decrease rapidly with depth. A protruding seamount disturbs the water flow, causing eddies of varying size (sub-mesoscale to mesoscale), internal waves, turbulent mixing and upwelling. A specific seamount-associated eddy is known as a Taylor column (or sometimes Taylor cap), which is anticyclonic and stationary over the summit, and it tends to retain small particles such as plankton and larvae. Such physical processes induce vertical movement of deeper, nutrient-rich water towards the sea surface which, given sufficient light, can enhance local plankton populations, and result in seamounts being aggregation areas for micronekton feeding (Lavelle and Mohn, 2010). The small fish in turn fall prey to predation by cephalopods, tuna, sharks and marine mammals, plus seabirds when the features are notably shallow. Other factors including water temperature, the depth of the upper mixed layer (and wind) and the extent of stratification, all play a role in shaping the benthic and pelagic ecosystems around seamounts.

The clear water conditions in the open ocean allow photosynthesis at greater depths than around continental shelves, so coralline algae for example can live at depths of 270 m (Littler et al., 1986). However, as depth increases beneath the upper sunlit layers of the ocean, current velocities and temperatures decrease, creating a different environment for the benthos. Evolving over millions of years, seamounts seem to have become isolated habitats that support communities high in endemism (Rogers, 1994; Tyler et al., 1995; Parin et al., 1997; Richer de Forges et al., 2000). Their isolated benthic and pelagic ecosystems make seamounts biological hotspots, stopping points for migrating animals such as whales, and stepping stones for the dispersion of biota across ocean basins. The position of a seamount relative to current systems, landmasses and latitude will influence dispersion, connectivity and ambient water properties.

# 1.3. Ridges and seamounts in the South West Indian Ocean

As stated by Roberts et al. (2020), most seamounts in the Indian Ocean are on the western side of the basin, notably along the South West Indian Ridge (SWIR). Fishers for decades have explored and fished the numerous seamounts on this ridge, first Soviet fleets, then French and Asian fleets in the 1970s and 1980s (Clark et al., 2007; Rogers et al., 2017). More recently, since 1990, the tuna longline fishery, mostly working from Réunion Island (Evano and Bourjea, 2012), has focused on a region south and east of Madagascar, where productivity seems to be enriched, a statement supported by studies on seabirds (Pinet et al., 2012). The region south of Madagascar overlies the Madagascar Ridge, an impressive bathymetric feature that to date has received little scientific attention because of its remoteness.

Aligned longitudinally, the Madagascar Ridge extends south of the Madagascar landmass for some 1300 km ( $\sim$ 10 degrees of latitude; Figs. 1 and 2) with a width of  $\sim$ 400 km. Water depths over much of the ridge are between 2 and 3 km. The southern half of the ridge rises to the prominent Walters Shoal, one of a group of several deeper seamounts, but which itself

comes within 18 m of the surface (Fig. 2b). Its flat summit is rather bare and covered with massive blocks of calcareous coraline algae (Bouchet P., pers. comm.). The northern part of the Ridge likewise consists of a cluster of seamounts shallower than 750 m. One of these, referred to in this study as the MAD-Ridge seamount, rises to a depth of 240 m below the sea surface (27.5°S, 46.25°E; Roberts et al., 2020). The western side of the Madagascar Ridge has a steep scarp that runs down into the 5-km-deep Mozambique Basin. The slope of the eastern flank is gentler, leading into the 5–6-km-deep Madagascar Basin. South of Walters Shoal, the water depth increases rapidly to more than 3000 m, whereupon, the 4000 m isobath joins the SWIR. Even with the northern and southern seamount clusters, the ridge is mostly flat-topped and covered by 0.5–1.0 km of undisturbed sediments (Goslin et al., 1980).

# 1.4. Regional oceanography

The Madagascar Ridge lies in a region of the southern Indian Ocean where the Subtropical Anticyclonic Gyre forms the general background circulation (Fig. 1a; Stramma and Lutjeharms, 1997; Lutjeharms, 2006), circulation portrayed by the baroclinic volume flux field over the upper 1000 m. Closure of the Subtropical Gyre has not yet been completely resolved (Pollard and Read, 2017). The gyre includes the powerful Agulhas Current (AC) as the major western boundary current (Fig. 1b). This flow retroflects at the southern tip of Africa, and mostly flows back east as the Agulhas Return Current (ARC), undergoing a series of semi-permanent meanders between 37°S and 41°S just north of the Subtropical Front (STF). The ARC weakens towards the east as transport peels off to the north (Stramma and Lutjeharms, 1997; Lutjeharms, 2007), then turns west to close the anticyclonic gyre. Northward leakage from the ARC also occurs in the form of cyclonic eddies that regularly form and break away, moving west (Pollard and Read, 2017). The westward recirculation within the Southwest Indian subgyre flows across the Madagascar Ridge.

The circulation south of Madagascar is complex and dominated by the strong South East Madagascar Current (S-EMC; Nauw et al., 2008). Similar to the situation for the AC, Lutjeharms (2007) suggested that the S-EMC undergoes an eastward retroflection once it becomes a free jet south of the landmass. Mesoscale eddies are formed there, which then propagate west towards southern Africa, where they merge with the upper reaches of the AC (Halo et al., 2014; Braby et al., 2016; de Ruijter et al., 2004). Ridderinkhof et al. (2013) demonstrated that much of this propagating turbulence is in the form of dipoles. Quartly et al. (2006) suggested that the retroflection at the end of the S-EMC is not a permanent feature. Siedler et al. (2006, 2009), on the basis of climatological altimetry data, proposed that the South Indian Ocean Countercurrent (SICC) was an eastward extension of the S-EMC retroflection. Palastanga et al. (2007) observed the SICC to extend to 100°E, and Siedler et al. (2009) suggested that up to 40% of SICC waters originate in the S-EMC.

Not much is known of the circulation south of the S-EMC retroflection area. Read and Pollard (2017) suggested that integrated westward transport between Madagascar and 37°S accounts for 50 Sv, which added to 25 Sv from the S-EMC, is sufficient to account for the total AC transport of 70  $\pm$  21 Sv, i.e. that it is a slow background flow. Observations from altimetry data show, superimposed on this background, that the southern part of the Madagascar Ridge is regularly affected by low-intensity eddies that propagate westwards (Read and Pollard, 2017).

# 1.5. Aims of this paper

The MADRidge Project (Roberts et al., 2020) was established in 2016 to further understand the pelagic ecosystems potentially supporting the productivity observed over the Madagascar Ridge and east of Madagascar. Three prominent shallow seamounts were selected for scientific investigation: two on the Madagascar Ridge, the Walters Shoal (18 m below the surface) and MAD-Ridge (240 m), and one east of

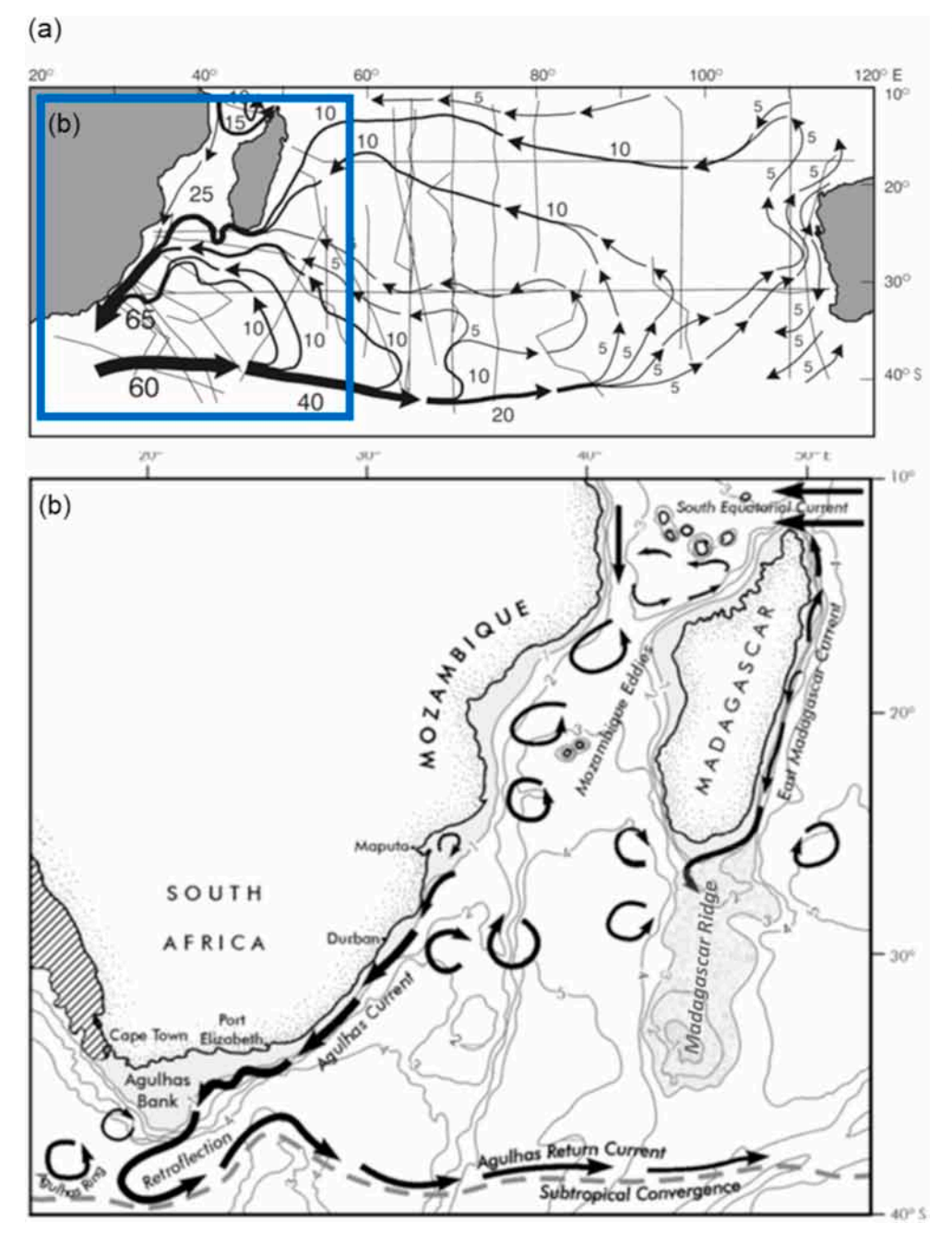


Fig. 1. (a) The South Western Indian Ocean subgyre forms the background circulation to the SWIO region (blue box). This is portrayed by the baroclinic volume flux field over the upper 1000 m (after Stramma and Lutjeharms, 1997). Transport volumes are in 10<sup>6</sup> m<sup>3</sup> s<sup>-1</sup>. (b) Schematic showing the major oceanographic features of the SWIO (adapted after Lutjeharms, 2006). The shaded bathymetry south of Madagascar identifies the Madagascar Ridge. (For interpretation of the reader is referred to the Web version of this article.)

Madagascar, La Pérouse (60 m), which rises from the abyssal plain. With the wish to help answer the question as to what shapes life on seamounts (see above), the present study was designed to provide a regional view of surface wind as a driver of upwelling and mixing, sea surface temperature (SST), mixed layer depth (MLD), and chlorophyll-a (hereafter chl-a) as key water column properties, and eddy kinetic energy (EKE) and currents as drivers of seamount processes and dispersion/connectivity. We attempt to provide a backdrop to the more-detailed ship-based, satellite and modelling investigations that supplement this study in the MADRidge Project special issue.

# 2. Data and methods

## 2.1. Study area and bathymetry

The GEBCO 2014 gridded bathymetry product (https://www.gebco.net/data\_and\_products/gridded\_bathymetry\_data/) was used to display

the bathymetry of the Madagascar Ridge, the two prominent seamounts Walters Shoal and MAD-Ridge, and the broader surroundings in the region, shown in Fig. 2). The product consists of a global terrain model for ocean and land at 30 arc-second intervals. Actual depths for the three prominent seamounts (including La Pérouse) were obtained from cruise surveys (see Roberts et al., 2020, for further detail).

## 2.2. Virtual moorings

As shown in Fig. 2, seven (numbered 1–7) 'virtual mooring' (VM) deployment points were selected along the Madagascar Ridge to investigate the circulation dynamics along it, including the MAD-Ridge seamount (VM 2) and the Walters Shoal (VM 6). At each location, time-series of absolute geostrophic velocity based on altimetry data were extracted (grid point) for four years (2011–2014). Position and depths at each VM position 1–7 are: VM 1 (46.25°E, 26.5°S; 1820 m), VM 2 (46.25°E, 27.5°S; 236 m), VM 3 (46.25°E, 28.5°S; 3170 m), VM 4

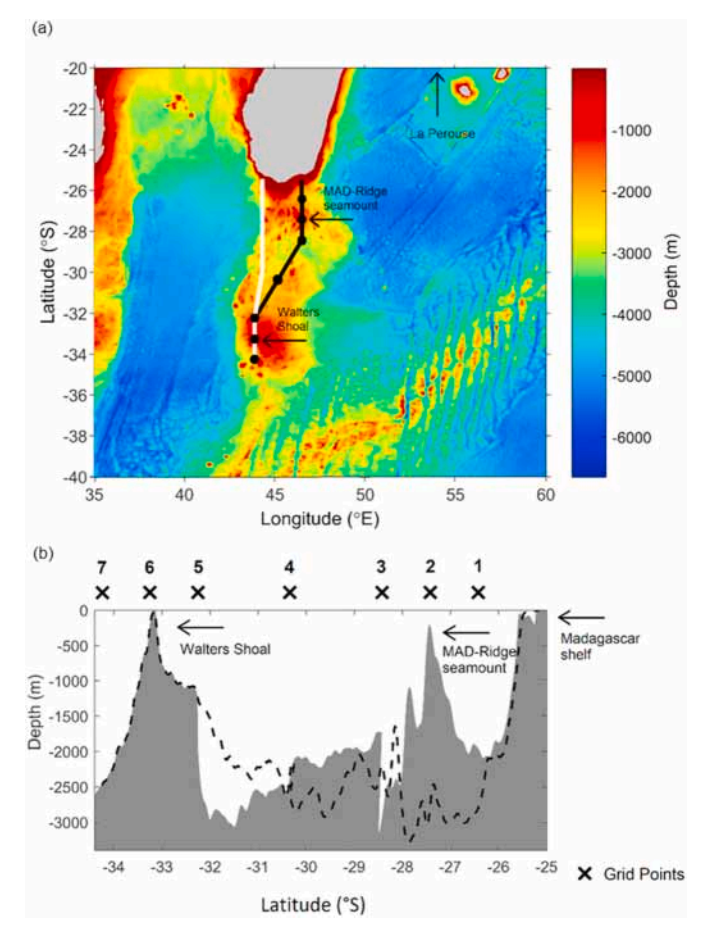


**Fig. 2.** (a) Bathymetry of the Madagascar Ridge (Gebco 2014 product) with two longitudinal transects (white and black). The seven black dots indicate the positions of the virtual moorings (VMs) referred to in text. (b) Vertical cross-sections of the bathymetry along these transects. The dashed line is along the white transect. Grey shading is along the black mooring line. Crosses along the top depict the positions of the virtual moorings (numbered), and serve as grid points to extract altimetry data.

(45.13°E, 30.38°S; 2520 m), VM 5 (44°E 32.25°S; 1200 m), VM 6 (44°E, 33.25°S; 18 m) and VM 7 (44°E, 34.25°S; 2330 m).

# 2.3. Altimetry data

Merged, daily interpolated, delayed time (DT), altimetry data gridded at '4° resolution were used (1993–2016). This product is produced by Ssalto/Duacs and is distributed by Copernicus Marine Environment Monitoring Service (CMEMS) (http://marine.copernicus.eu/). Mean absolute dynamic topography (MADT) data are used to highlight the circulation dynamics using climatologies over the Madagascar Ridge. Mean EKE is derived from the MADT data over a specified domain in the South West Indian Ocean (SWIO) that includes the entire Madagascar Ridge. This is calculated using the equation

$$\overline{EKE} = \frac{1}{2} \left( \overline{u_g^{\prime 2}} + \overline{v_g^{\prime 2}} \right),$$

where  $\bar{}$  implies a time-average over the period 1993–2016, and  $u_g^{'2}$  and  $v_g^{'2}$  are the zonal and meridional components of the surface geostrophic current anomaly computed directly from the MADT. The MADT data are also used to calculate the absolute geostrophic velocity at each of the seven VM points along the Madagascar Ridge for the four years 2011–2014.

For near-surface ocean current estimates, OSCAR (Ocean Surface

Currents Analyses Real-time) products are deemed to be superior to satellite altimeter-derived geostrophic currents, because the calculation is improved using satellite data and validation methods (for detail, see https://www.esr.org/research/oscar/oscar-surface-currents/). OSCAR, currents are averaged over the top 30 m of the ocean, and provided on a global  $\frac{1}{3}$ ° grid with a 5-day resolution dating from 1992 to present. OSCAR is generated by Earth Space Research (ESR). However, a comparison between OSCAR and MADT-derived products (Supplementary Material Fig. S1), showed only small differences in current direction and velocity at each mooring, with the OSCAR product being mainly lower in velocity by an average of 7 cm s<sup>-1</sup>. A comparison of MADT-generated geostrophic velocities at VM 6 with passing historical in situ surface drifters (Supplementary Material Fig. S2) indicated the MADT product to be on average 8 cm s<sup>-1</sup> slower. On the basis of these determinations, it was decided to use the MADT-derived geostrophic velocities herein. The absolute geostrophic velocities were also validated over the northern Madagascar Ridge against cruise-collected S-ADCP data (see Fig. 3 of Vianello et al., 2020). Demarcq et al. (2020) used the same product.

## 2.4. Wind, SST, MLD and chlorophyll data

Wind data obtained from <a href="http://www.remss.com/measurements/ccmp/were">http://www.remss.com/measurements/ccmp/were</a> used to produce a climatology (1993–2015) with a spatial resolution of ½° and a temporal resolution of 6 h. These data are configured to represent a measurement 10 m above the ocean surface, and comprise a cross-calibrated, multi-platform (CCMP) gridded product that uses a combination of radiometer wind speeds, QuikSCAT and ASCAT scatterometer wind vectors, moored buoy and model wind data, and is a Level 3 ocean vector wind analysis product (Atlas et al., 2011).

SST data obtained from http://data.remss.com/SST/daily/were used to produce a climatology (1998–2014) with a spatial resolution of 9  $\times$  9 km and a temporal resolution of 1 day. This 9 km microwave optimally interpolated SST product combines the through-cloud capabilities of the microwave data (25  $\times$  25 km resolution), with the better spatial resolution (9  $\times$  9 km) and near-coast capability of the infrared SST data. An interpolated algorithm is implemented to homogenise the resolution of the combined product.

The MLD data were downloaded from http://www.ifremer.fr/cerw eb/deboyer/mld/home.php) and used to produce a climatology (1985–2009) with a spatial resolution of  $2^{\circ}$  and a temporal resolution of 1 month. The criterion used to obtain the MLD was: MLD = depth where  $(\theta = \theta_{10 \text{ m}} - 0.2 \, ^{\circ}\text{C})$ , according to de Boyer Montégut et al. (2004).

Chlorophyll-a data obtained from Hermes Globcolour (http://hermes.acri.fr/) were used to produce a climatology (1998–2016) with a spatial resolution of 4  $\times$  4 km and a temporal resolution of 1 day.

# 3. Results

#### 3.1. Regional climatology maps

## 3.1.1. Surface winds

Fig. 3a and b shows the summer (a) and winter (b) climatology (1993–2015) for the regional wind field inclusive of the Madagascar Ridge. In this study, summer refers to December, January and February and winter to June, July and August. Colours represent wind speed, and the direction is shown by the white arrows (vectors). The black horizontal lines depict the latitude of the MAD-Ridge seamount and Walters Shoal. In austral summer, the wind direction is easterly along the entire ridge (trade winds), with speeds increasing from 6.5 to 8.5 m s $^{-1}$  in the northern part. The wind field deflects around southern Madagascar, but there is also a permanent local acceleration 'hotspot' off the southeast coast. This extends to the MAD-Ridge seamount and is stronger during winter. This hotspot has also been noted by Collins et al. (in prep.). During summer, the westerly wind belt is found south of 36°S and does not reach the ridge, but in winter it moves north and impinges on the

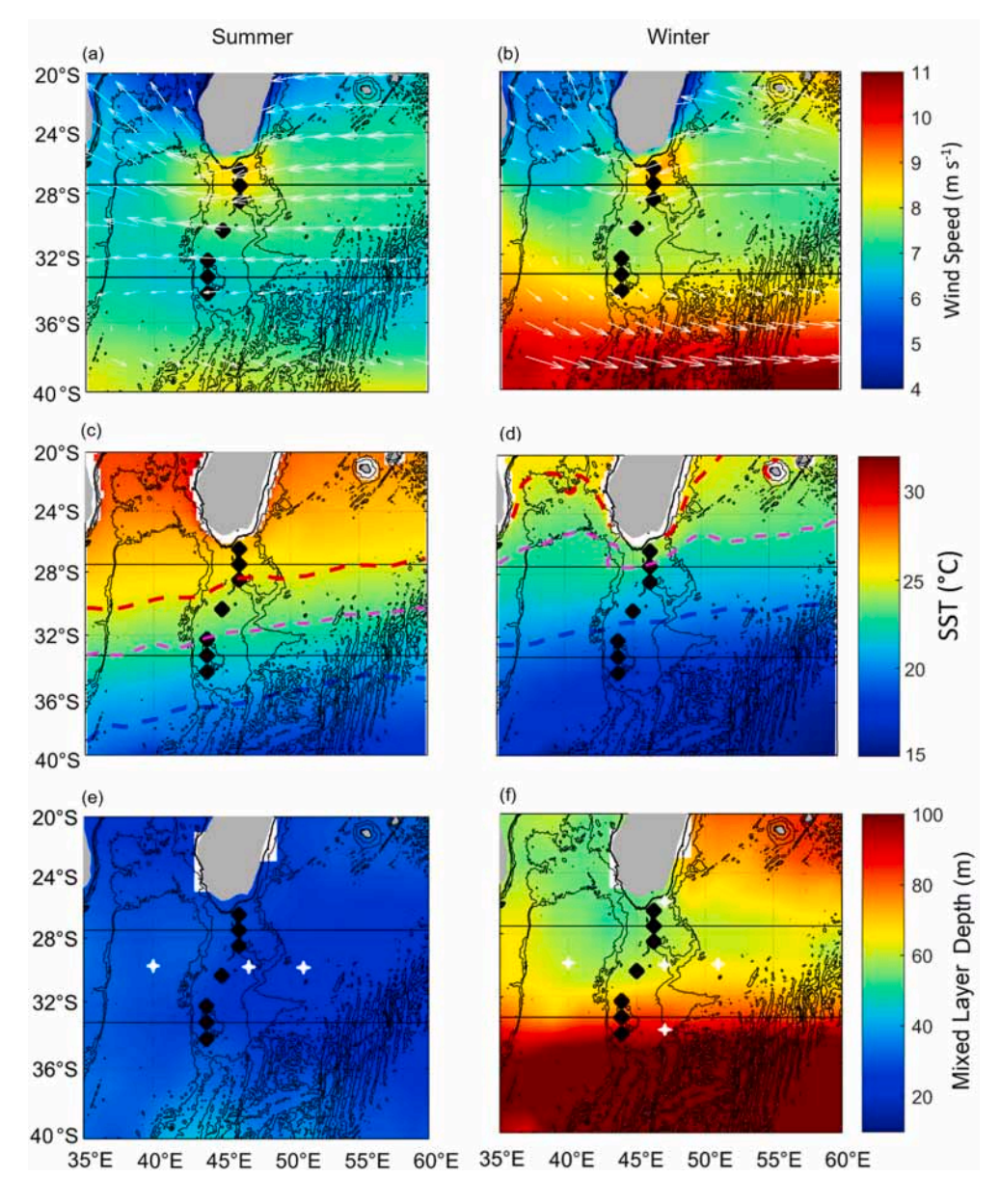


Fig. 3. Summer and winter wind field and ocean properties in the greater region of the Madagascar Ridge: (a) and (b) Surface winds (1993-2015), (c) and (d) SST (1998-2014), (e) and (f) MLD (1985-2009), (g) and (h) EKE (1993–2016), (i) and (j) Chl-a (1998-2016). The two horizontal black lines indicate the latitudes of the MAD-Ridge seamount (27.5°S) and Walters Shoal (33.25°S), and the black diamonds indicate the seven virtual moorings along the Madagascar Ridge. For convenience, the 20 °C (blue), 23 °C (pink) and 25 °C (red) isotherms are shown in (c) and (d). White 'X's are reference points in the text. All maps have a GEBCO 2014 bathymetry overlay. (For interpretation of the references to colour in this figure legend, the reader is referred to the Web version of this article.)

southern reaches of the ridge, including the Walters Shoal (Rubin and van Loon, 1953), bringing with it stronger winds of >9 m s<sup>-1</sup>. Winds near La Pérouse at  $20^{\circ}$ S tend to be moderate (6–7 m s<sup>-1</sup>) year-round.

# 3.1.2. Sea surface temperature

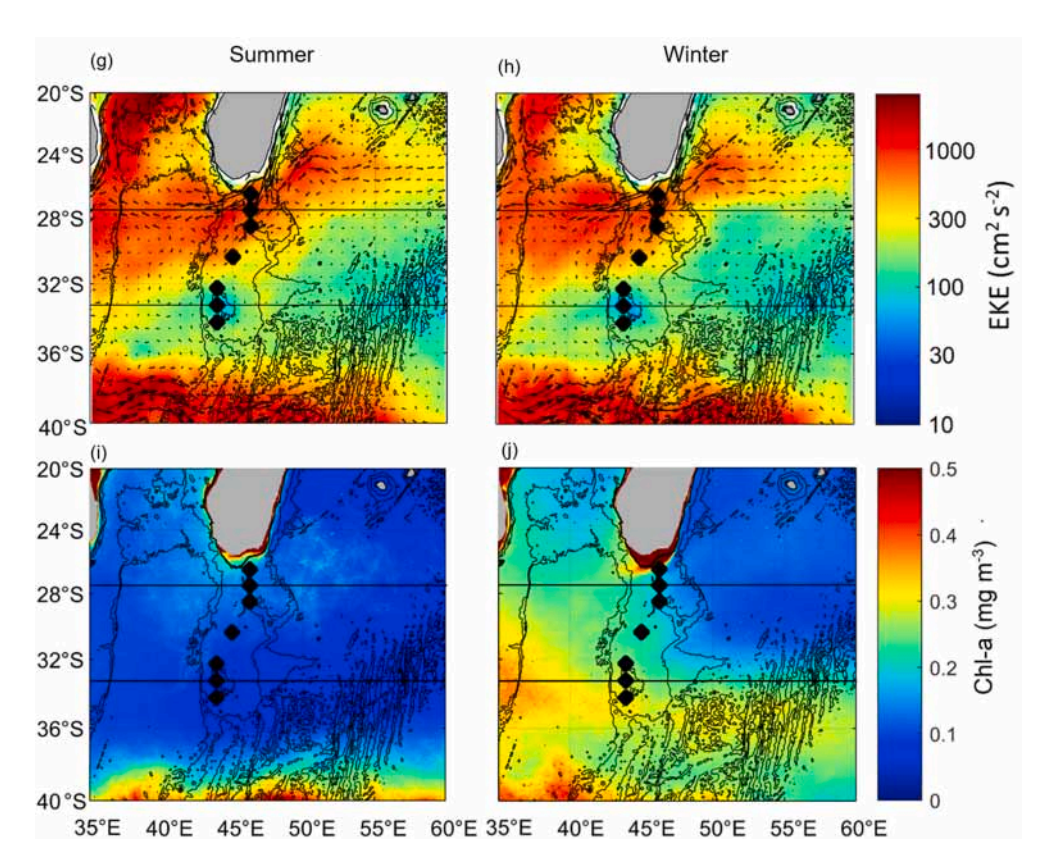
The regional seasonal SST climatology (1998–2014) for the domain that interests us here are depicted in Fig. 3c and d. Most notable in these maps is the seasonal meridional movement of surface isotherms, typified by the 20, 23 and 25 °C contours (shown). There is also a permanent zonal SST gradient with warmer temperatures in the west being farther south than in the east, no doubt a consequence of the influence of the AC. Highest summer SSTs in this regional domain, around 28–30 °C, are found in the Mozambique Channel, with SSTs east of Madagascar being some 2 °C cooler. This zonal disparity is less during winter, when SSTs cool to 24–25 °C either side of Madagascar. Over the ridge, the 23 °C isotherm (pink) migrates south from its winter position over the MAD-Ridge seamount to the southern part of the ridge. This implies that MAD-Ridge has a long-term average summer SST of 25.8  $(\pm 0.7)^{\circ}$ C, which then drops in winter to 23  $(\pm 1.0)^{\circ}$ C. South, at the Walters Shoal,

the long-term average SST ranges from 21.8 ( $\pm 0.6$ )°C in summer to 18.4 ( $\pm 0.5$ )°C in winter, indicating an all-round 3 °C (on average) difference in surface temperature regimes. For comparison, the seasonal SST range at La Pérouse is from 27.7 ( $\pm 0.8$ )°C in summer to 24.8 ( $\pm 0.9$ )°C in winter.

## 3.1.3. Mixed layer depth

The seasonal MLD climatology (1985–2009) are shown in Fig. 3e and f. There are large seasonal differences. During summer, the MLD varies marginally with a 4-m range along the Madagascar Ridge and throughout the selected domain. For example, the MLD at  $30^{\circ} S, 47^{\circ} E$  (white 'X') on the ridge is  $24~(\pm 4)$  m. To the west (30°S, 40°E) in the Mozambique Basin, it is  $30~(\pm 5)$  m, and to the east on the same latitude (30°S, 51°E) it is  $24~(\pm 4)$  m. In the far north near La Pérouse, summer MLD is  $29~(\pm 7)$  m. During winter, however, greater contrasts exist between north and south, ranging from nearly 120~m at  $40^{\circ} S$  to 58~m near the MAD-Ridge seamount. North of there, the MLD deepens again to  $84~(\pm 15)~m$  at  $20^{\circ} S$  near La Pérouse. Note also the stark difference between the eastern side of Madagascar and the Mozambique Channel, where the

Fig. 3. (continued).



MLD is shallower, between 55 and 60 m, about the same as the northern Madagascar Ridge. The deep southern MLD values are attributable to the northward migration of the westerly wind belt seen in Fig. 3a and b. Along the Ridge, the MLD deepens by some 40 m from 58 ( $\pm 17$ ) m at 26°S, 47°E (white 'X') near the MAD-Ridge seamount, to 65 ( $\pm 14$ ) m midway at 30°S, 47°E, to 100 ( $\pm 23$ ) m at 34°S, 47°E in the south. Relatively, there is only a slight west–east MLD gradient across the Ridge, e.g. west of the ridge at 30°S, 40°E (white 'X'), the MLD is 63 ( $\pm 16$ ) m, and east of the ridge at 30°S, 51°E (another white 'X'), it is 69 ( $\pm 9$ ) m.

#### 3.1.4. Eddy kinetic energy

Fig. 3g and h shows the EKE climatology (1993-2016) for the Madagascar Ridge region. The turbulent eddy areas (i.e.  $>1000 \text{ cm}^2 \text{ s}^{-2}$ ) are clearly revealed, on the western side of the Mozambique Channel (e. g. Roberts et al., 2014), south of the Madagascar landmass where the S-EMC terminates (e.g. Siedler et al., 2009) and along the boundary of the ARC (STF) near 40°S (e.g. Read and Pollard, 2017). The central region of the SWIO gyre that overlaps with the southern Madagascar Ridge has the lowest EKE. Around these features, there is very little difference between summer and winter regimes in terms of EKE (at least in this climatological analysis). In terms of the MADRidge Project, this demonstrates that the MAD-Ridge seamount and Walters Shoal are positioned in completely contrasting EKE regimes. For both summer and winter, Walters Shoal has a low EKE climatology of around 50 cm<sup>2</sup> s<sup>-2</sup>, whereas the MAD-Ridge seamount at the tail end of the S-EMC has a much higher EKE of some 850 cm<sup>2</sup> s<sup>-2</sup> being in the main high EKE corridor. Also, although the EKE is very low on the southern reaches of the ridge, eddies are still found there, albeit infrequently and with low sea surface height (SSH) (Read and Pollard, 2017). La Pérouse is situated in an area of intermediate EKE, with a mean summer value of 185 cm<sup>2</sup>  $s^{-2}$  and a mean winter value of 173 cm<sup>2</sup>  $s^{-2}$ .

#### 3.1.5. Surface chlorophyll-a

The surface summer and winter chl-a climatology (1998-2016) are shown in Fig. 3i and j. Summer experiences low values of  $\sim 0.1 \text{ mg m}^{-3}$ over much of the region. Exceptions are on the southern Madagascar shelf and in the south around 40°S, where the STF is found at that time of year. Note that the east Madagascar bloom, which appears at times between January and April, is not evident, no doubt a consequence of its intermittent nature (Srokosz et al., 2015; Dilmahamod et al., 2019). Throughout the year, the dominant high chl-a levels in this entire region are found on the Madagascar shelf, in winter on the mid-shelf at 45.35°E, 26°S, where the value is  $0.24 \pm 0.07$  mg m<sup>-3</sup>. This is associated with wind-driven coastal upwelling and the divergence caused at that time by the S-EMC (see also later, in Fig. 4). It is also worth noting that there is no chl-a signature for the eddy corridor south of the Madagascar shelf. On the Madagascar Ridge, the MAD-Ridge seamount has a climatological summer mean of  $0.14 \pm 0.04$  mg m<sup>-3</sup>, as does the Walters Shoal with its  $0.14 \pm 0.03 \ \text{mg m}^{-3}$ , further reinforcing the uniformity of the property. In winter, however, regional variation is apparent. Little changes in the central gyre east of Madagascar, as typified near La Pérouse, with its values of 0.07  $\pm$  0.02 mg m $^{-3}$  in summer and 0.12  $\pm$  $0.02 \text{ mg m}^{-3}$  in winter. Chl-a on the Madagascar shelf is higher at 0.54 $\pm$  0.21 mg m<sup>-3</sup>. South of 32°S, the mean winter chl-a begins to increase to values > 0.3 mg m<sup>-3</sup>, the highest mean values in the entire domain for all seasons. Not surprisingly, this overlaps with the deepening of the MLD shown in Fig. 3f, and the vertical mixing of nutrients from below. The winter mean over the Walters Shoal is  $0.26 \pm 0.04$  mg m<sup>-3</sup> and at MAD-Ridge 0.19  $\pm$  0.02 mg m $^{-3}$ . The elevated chl-a centred around 33°S and west of 40°E, where values rise between 0.3 and 0.4 mg m<sup>-3</sup>, presumably stems from both a shallower MLD and the dynamics of the ARC. A noteworthy point too is the enhanced chl-a west of the Madagascar Ridge, where the MLD remains deepest during winter.

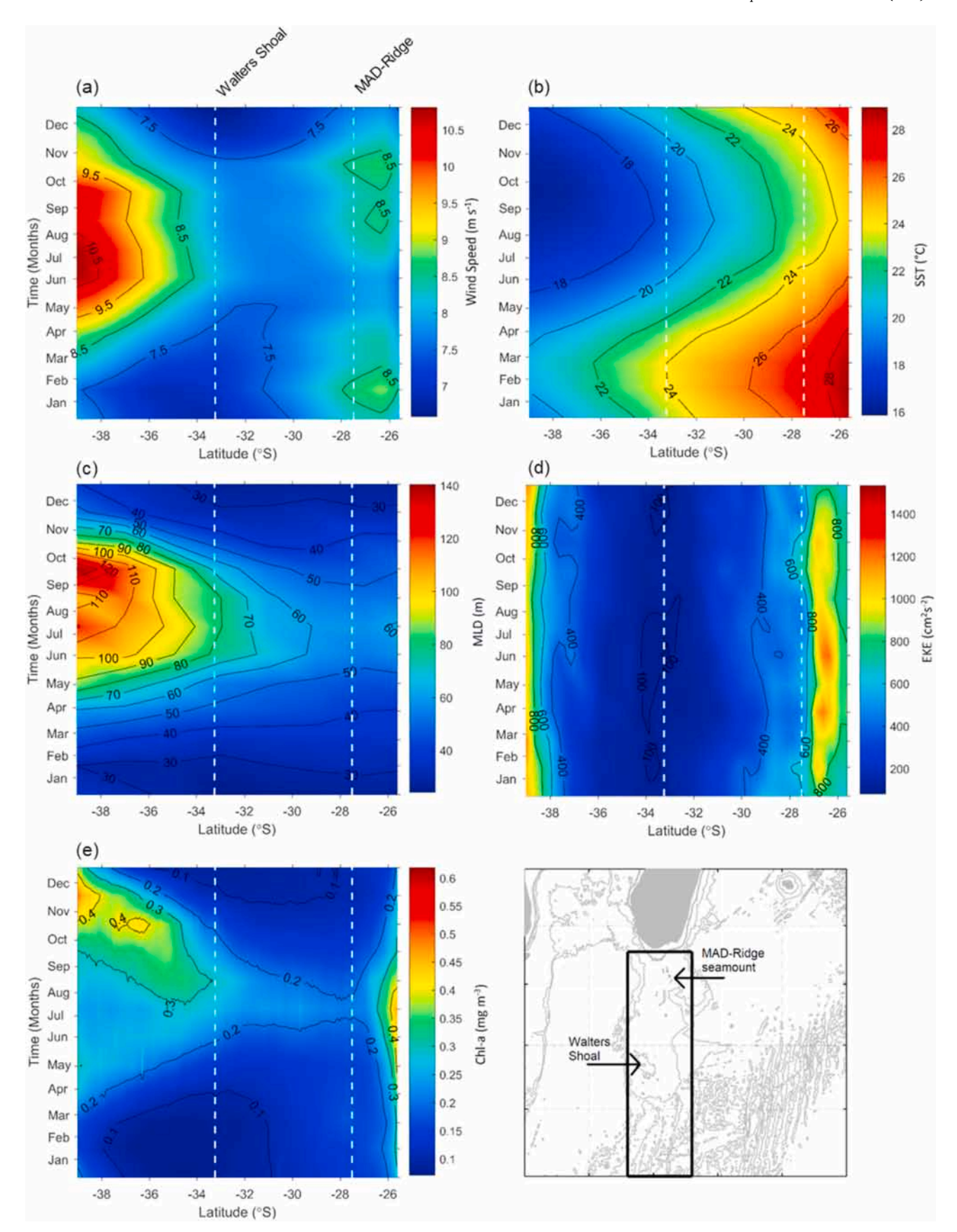


**Fig. 4.** Climatological Hovmoller plots detailing gradients of water properties along the Madagascar Ridge (averaged in the area between 43 and 48°E and 26–40°S, shown by the box in the bottom right plot): (a) surface winds, (b) SST, (c) MLD, (d) EKE, (e) chl-a.

#### 3.2. Monthly water property gradients over the Madagascar Ridge

As the Madagascar Ridge is the focus of the MADRidge Project, we now highlight, using Hovmoller plots, the mean monthly (seasonal) dynamics of these water properties along the ridge, averaged in the area between 43 and 48°E and 26 and 40°S (see box in Fig. 4), complementing the spatial information produced in Fig. 3. In the case of surface winds (Fig. 4a), the northward encroachment of the high velocity (>10 m s $^{-1}$ ) westerly wind belt starts in April, peaks in July, then subsides in October. To the north between 26 and 28°S, wind speed is bimodal, with maxima of 9 m s $^{-1}$  in February and November. These values correspond to the local acceleration south of the Madagascar landmass, observed in Fig. 3a and b, and highlights the fact that the small seasonal difference seen there is an artefact of the months chosen to represent summer and winter.

In the case of SST (Fig. 4b), a strong gradient (difference between 26 and 40°S) ranging between 6 and 9 °C is observed throughout the year along the ridge. This means that at Walters Shoal, SST ranges from 19 °C in September to 24 °C in February, and at MAD-Ridge, the range is 23 °C in September to 27 °C in February.

As would be expected, the MLD (Fig. 4c) along this transect shows a similar pattern to that of surface winds (Fig. 4a), being deeper (>100 m) south of 36°S in winter between June and October. During summer, the MLD is not dissimilar (30–40 m) along the Ridge, but it is deeper at Walters Shoal (i.e. 80 m) than at MAD-Ridge (55 m) in winter (July).

As already noted in Fig. 3, the EKE in this region is high immediately south of Madagascar as a result of the S-EMC, and also south of 38°S because of the boundary dynamics of the ARC. These are starkly portrayed in Fig. 4d too, but here we also see some intra-annual variability in the EKE climatology representing the mesoscale eddy activity south of Madagascar. The data highlight the period March–August as having either more eddies or more-intense eddies. The EKE arising from the ARC is consistently intense and shows little spatial intra-annual variability. Between these extremes, the remainder of the Madagascar Ridge has low EKE throughout the year. Similar to Fig. 3g and h this plot highlights the contrasting high vs. low energy environments between MAD-Ridge and Walters Shoal (i.e. low-vs. high-speed currents).

Fig. 4e shows low levels of chl-a over the ridge, ranging from <0.1 mg m $^{-3}$  during summer to a little over 0.2 mg m $^{-3}$  in July. Chl-a on the Madagascar shelf, in terms of climatology, peaks ( $\sim$ 0.4 mg m $^{-3}$ ) around July and is lowest ( $\sim$ 0.2 mg m $^{-3}$ ) between October and January (we also draw attention here to the work by Demarcq et al., 2020, for the Madagascar shelf). South of 34°S, the emergence of the spring bloom is conspicuous between September and December, with the southern part of the Madagascar Ridge showing earlier emergence than farther south near the STF.

#### 3.3. Ocean circulation (geostrophic currents)

## 3.3.1. Region view

Fig. 5 shows the summer and winter climatologies (1993–2016) of the geostrophic circulation in the greater vicinity of the Madagascar Ridge. The southern study boundary has been extended to show the ARC. Eddies particularly dominant on the western side of the Mozambique Channel, over the northern Madagascar Ridge (Halo et al., 2014; Vianello et al., 2020), and along the boundary of the ARC are smoothed in these climatologies. The dominant currents in the region, the EMC, the AC and the ARC, along with their characteristics, are conspicuous year-round, with little seasonality in position and speed, although the EMC tends on average to be stronger in winter than in summer (i.e. 60 vs. 70 cm s $^{-1}$ ). Currents over the central and southern parts of the Ridge have on average low velocities ( $\sim 15~{\rm cm~s}^{-1}$ ), with no coherence in the climatological mean direction, and they lack seasonality.

## 3.3.2. Geostrophic currents over the Ridge (virtual moorings)

Details on the variability of the geostrophic currents along the Madagascar Ridge (shown in Fig. 5) are now given in Fig. 6. These consist of 4-day vector time-series plots over a time-span of 365 days (i. e. a vector every 4 days) for each of the VMs shown in Fig. 2. Four years of data are plotted (2011–2014).

It is clear that geostrophic velocities generally decrease from north to south (i.e. VM 1 to VM 7). As seen by the steady southwesterly vectors in both annual maps (Fig. 5) and the 4-year time-series (Fig. 6), VM 1 is firmly positioned in the S-EMC; there are only a few occasions when this pattern deviates. Velocities generally range from 30 to 90 cm s $^{-1}$  (see Table 1 for more detail), but can reach 118 cm s $^{-1}$  (e.g. Day 161, 2013).

Velocities drop at VM 2 (MAD-Ridge), ranging between 10 and 70 cm s $^{-1}$ , but on occasion can reach 94 cm s $^{-1}$  (e.g. Day 46, 2011). The direction of the current is far less constant and with a strong eastward component. As demonstrated in Vianello et al. (2020), the MAD-Ridge seamount is similarly in a zone of high mesoscale activity, with eddies occurring 93.8% of the time (1993–2016). Certainly, the passing of mesoscale eddies, with their rotating currents, is evident in the 2011 time-series, but the more steady northeastward current from mid-2012 to mid-2014 suggests the presence of SICC.

Velocities at VM 3 have a comparable range to those at VM 2 (i.e. 10– $60\,\mathrm{cm\,s^{-1}}$ ) and there is little coherence in the current direction there. Currents can also on occasion reach 86 cm s<sup>-1</sup> (Day 41, 2011). The sequential rotation of vectors indicates that this position is still strongly influenced by the passing EMC-generated eddies. These do not always correlate with the currents for the same period at VM 2, especially between mid-2012 and mid-2014, suggesting that the retroflection of the EMC is restricted to the area of VM 2.

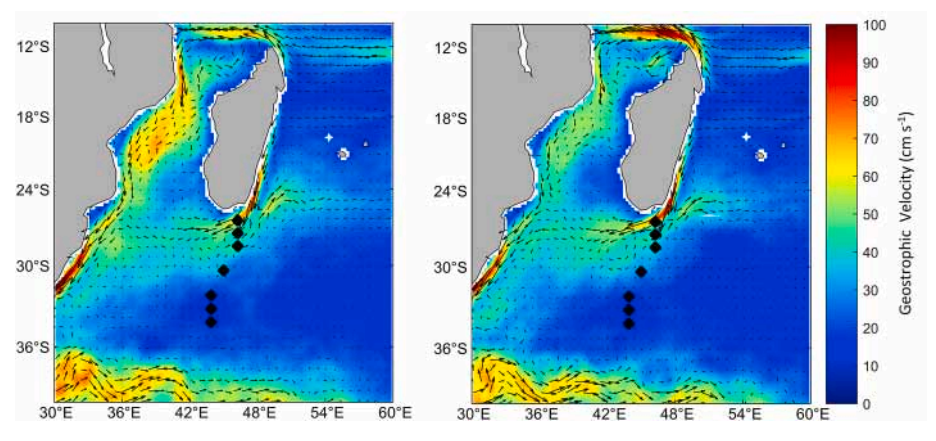


Fig. 5. Climatology of the surface circulation in the vicinity of the Madagascar Ridge in (a) summer and (b) winter.

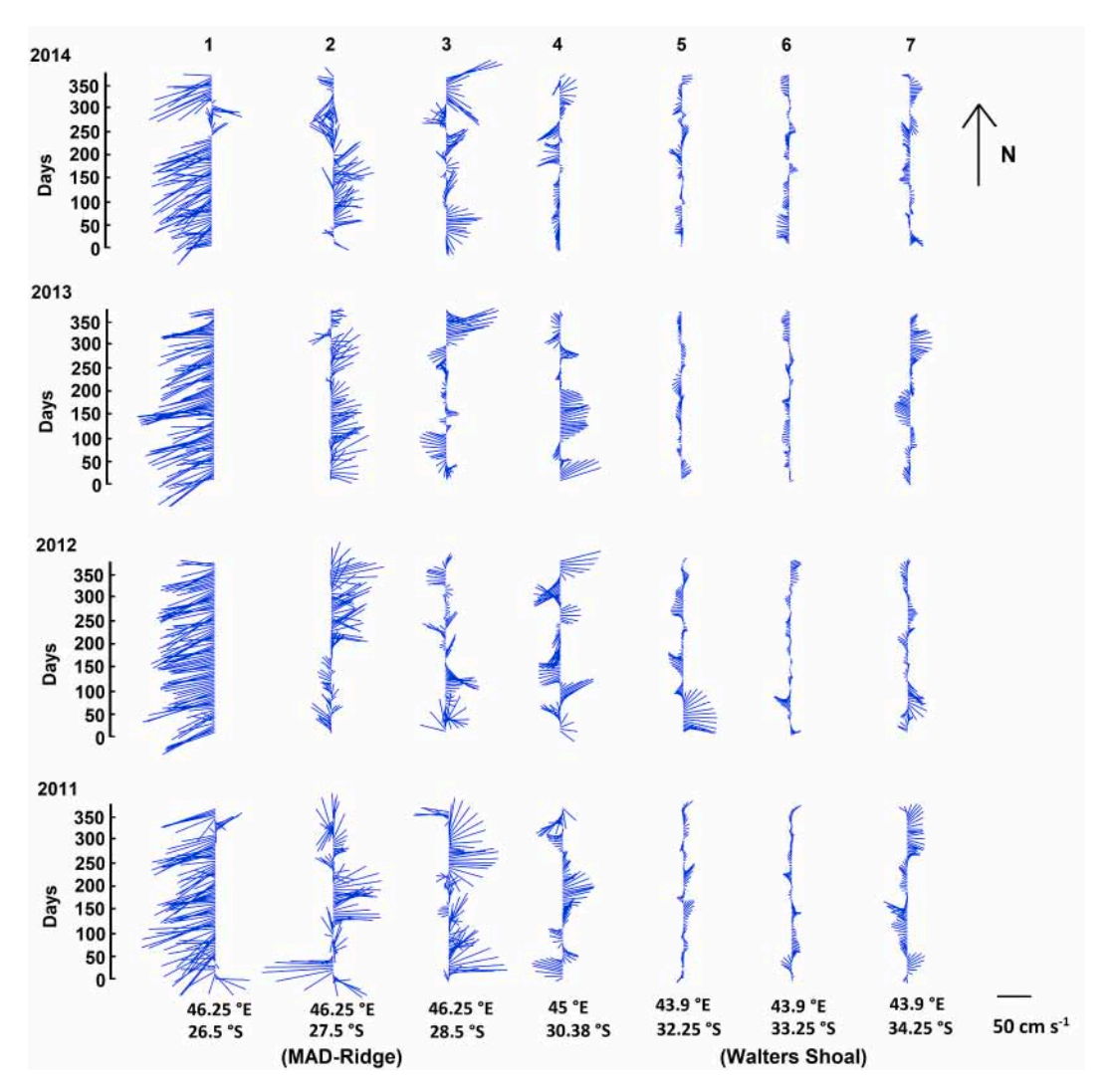


Fig. 6. Four-day vector time-series of geostrophic currents between 2011 and 2014 for the seven virtual mooring sites (numbered) along the Madagascar Ridge, as shown on Fig. 2. The scale is given at the bottom right.

**Table 1** Geostrophic current statistics for the virtual moorings (VM 1–7) over a 4-year period.

Mooring	2011		2012		2013		2014	
	Max (cm s <sup>-1</sup> )	Mean (cm s <sup>-1</sup> )	Max (cm s <sup>-1</sup> )	Mean (cm s <sup>-1</sup> )	Max (cm s <sup>-1</sup> )	Mean (cm s <sup>-1</sup> )	Max (cm s <sup>-1</sup> )	Mean (cm s <sup>-1</sup> )
VM 1	104.7	$60.5 \pm 22.9$	107.6	59.9 ± 20.7	118.1	$59.4 \pm 25.6$	114.4	$50.4 \pm 26.7$
VM 2	94.3	$38.8 \pm 18.5$	73.4	$33.4\pm17.5$	63.6	$27.4 \pm 11.6$	74.8	$32.7\pm17.0$
VM 3	86.2	$40.9 \pm 22.0$	67.1	$24.6\pm15.8$	74.0	$22.6\pm15.0$	79.7	$31.3\pm17.9$
VM 4	61.2	$24.3\pm13.6$	59.3	$31.1\pm11.1$	66.7	$21.6\pm14.3$	47.4	$14.7 \pm 9.1$
VM 5	32.2	$13.4 \pm 6.5$	70.0	$20.1\pm17.9$	20.1	$10.7 \pm 4.8$	32.4	$12.4 \pm 6.5$
VM 6	20.6	$9.4 \pm 4.6$	24.5	$7.8 \pm 4.8$	17.4	$8.1\pm3.4$	21.3	$9.8 \pm 5.2$
VM 7	35.9	$17.9 \pm 6.9$	40.5	$11.4 \pm 7.8$	31.8	$12.5\pm7.3$	27.5	$10.6 \pm 5.4$

Currents at VMs 4–7 all show similarly rotating vector patterns indicative of passing mesoscale eddies (Quartly et al., 2006), albeit with decreasing velocities towards the Walters Shoal (VM 6), i.e.  $\sim\!25~{\rm cm~s^{-1}}$  reducing to  $\sim\!8~{\rm cm\,s^{-1}}$ . As pointed out in Fig. 3h, Walters Shoal is located in a region of very low EKE.

Fig. 7 shows rose diagrams for the seven VMs using the full altimetry dataset from 1993 to 2016 and provides convenient summaries of the mooring currents. The unidirectional southwesterly current observed in the 4-year time-series at VM 1 is clear, but there is no coherence in direction at the other 6 VMs. The decrease in velocities towards Walters Shoal is also conspicuous, as is the slight increase farther south at VM 7.

The dominant northeast currents at VM 2 and VM 3 are evident.

# 3.3.3. Monthly current climatology over the Madagascar Ridge

Fig. 8 expands the knowledge gained from the 4-year records at the mooring sites (Fig. 7) and provides a full monthly climatology (1993–2016) of the geostrophic currents over the Madagascar Ridge (25 - 37°S). This serves to highlight gradients too, as shown for properties in section 3.2 above. Note the scale change indicated by the black line in Fig. 8. The strong southwestward currents shown in Figs. 6 and 7 north of the Mad-Ridge seamount are seen in Fig. 8 as being very persistent, signalling the dominance of the S-EMC year-round. The northeast

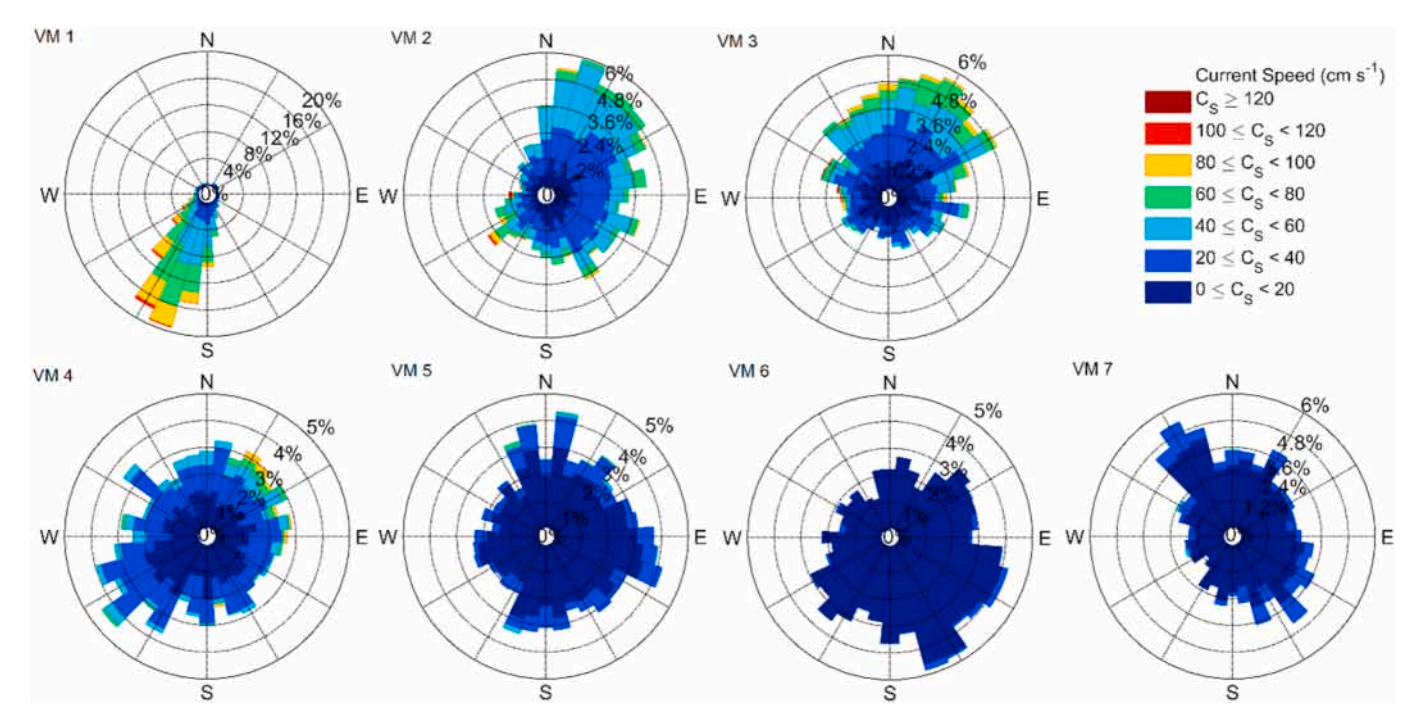


Fig. 7. Rose diagrams of geostrophic currents between 1993 and 2016 at virtual moorings (VMs) 1-7.

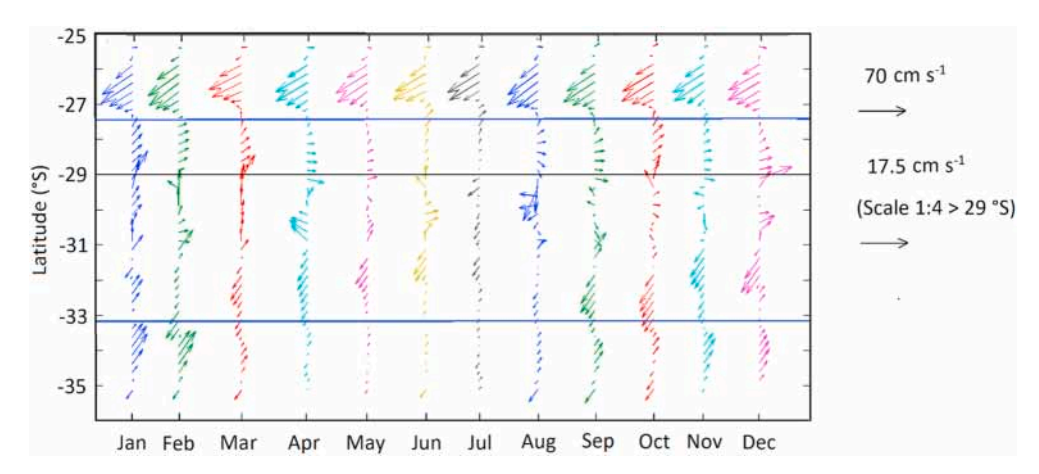


Fig. 8. Monthly mean climatology of geostrophic currents along the Madagascar Ridge for the period 1993–2016. Blue lines indicate the position of the MAD-Ridge seamount (27.5°S, top) and Walters Shoal (33.25°S, bottom). The black line indicates a change of scale for current strength, indicated in the key to the right. (For interpretation of the references to colour in this figure legend, the reader is referred to the Web version of this article.)

climatological currents seen between MAD-Ridge and  $29^{\circ}S$  (the black line), would suggest the presence of the S-EMC retroflection, fitting the literature, but those in Fig. 8 show a seasonality with stronger currents in summer (December–March) and weaker ones in winter (May–July). A similar pattern is also observed south of Walters Shoal, but with a longer period of weak currents during winter (March–August). This is interesting, because it is the opposite pattern to that of wind and MLD shown in Fig. 3, which are both influenced by the seasonal migration of the westerly wind belt.

As noted above, Walters Shoal is located in a region of particularly weak currents. North of it, to  $29^{\circ}S$  (the black line), the great variability in currents highlighted above (Fig. 7), is unambiguous with few obvious patterns, the exception possibly being just above  $33^{\circ}S$  between September and December, when there appears to be a distinct southwesterly flow.

#### 4. Discussion

# 4.1. Gradients and surface layer properties at the seamounts

As pointed out above, life on seamounts is structured by factors such as depth, horizontal and vertical gradients of water column properties, latitudinal diversity gradient (LDG) and ocean circulation. We therefore wanted to provide a regional view of surface wind as a driver, SST, MLD and chl-a as key water column properties, and EKE and currents as drivers of seamount processes and dispersion/connectivity. Focus was therefore on the three regionally prominent shallow seamounts under investigation in the MADRidge Project, two on the Madagascar Ridge, Walters Shoal and MAD-Ridge, and the other, La Pérouse, farther north and east of Madagascar in the Madagascar Basin. The three span a distance of some 1500 km between 20 and 33°S.We summarise our results for wind, SST, MLD, chl-a and EKE in Table 2, to look for similarities or differences between the three seamount environments. It is important to remember that these results are climatological means. Combined with

Table 2 Grid point extraction and summary of parameters from the climatological maps shown in Figs. 3 and 5 at the three seamounts for summer (DJF) and winter (JJA). Values are means  $\pm$  standard deviation. Note that mean current speed here is calculated on the magnitude of the current (not direction). The seasonally averaged velocity vector is considerably lower due to variability of the current direction (see Fig. 7) at MAD-Ridge (i.e., 4.4 cm  $s^{-1}$  / 12.7 cm  $s^{-1}$  for summer / winter seasons respectively) and the at two other seamounts: Walters Shoal (3.1 cm  $s^{-1}$  / 2.8 cm  $s^{-1}$ ) and La Pérouse (2.1 cm  $s^{-1}$  / 5.2 cm  $s^{-1}$ ).

Variable	MAD-Ridge	MAD-Ridge		Walters Shoal		La Pérouse	
	Summer	Winter	Summer	Winter	Summer	Winter	
Wind Speed (m s <sup>-1</sup> )	8.4 ± 1.0	$8.5 \pm 1.1$	$6.7 \pm 0.1$	$8.0 \pm 1.0$	$6.4\pm0.8$	$8.1 \pm 1.0$	
SST (°C)	$25.8 \pm 0.7$	$23.0\pm0.1$	$21.8 \pm 0.6$	$18.4 \pm 0.5$	$27.7\pm0.8$	$24.8 \pm 0.9$	
MLD (m)	$30 \pm 9$	$54\pm14$	$26\pm7$	$82\pm21$	$29\pm7$	$84\pm15$	
EKE $(cm^2 s^{-2})$	$856\pm13$	$851\pm17$	$56\pm 1$	$53\pm1$	$185\pm3$	$173\pm3$	
$Chl-a (mg m^{-3})$	$0.14 \pm 0.04$	$0.19 \pm 0.02$	$0.14\pm0.03$	$0.26\pm0.04$	$0.07\pm0.02$	$0.12\pm0.02$	
Current speed (cm s <sup>-1</sup> )	$41.7\pm18.2$	$43.2 \pm 21.2$	$11.1\pm1.2$	$10.7\pm1.2$	$19.4 \pm 3.8$	$19.3 \pm 4.4$	

those in Figs. 3 and 4, they show stark seasonally dependent differences along the Madagascar Ridge, and moreover along the whole range of the study domain (20–33°S). Surface wind showed local acceleration of the trade winds around the southern tip of Madagascar. This was also noticed by Collins et al. (in prep.), who suggest enhanced coastal upwelling and productivity on the shelf there. The productivity is seen in satellite observations being exported offshore in filaments that extend onto the Ridge, reaching at times the MAD-Ridge seamount. This was verified by Harris et al. (2020), who found substantial numbers of neritic fish larvae at MAD-Ridge. We also observed the seasonal northward migration of the westerly wind belt (strong winds) over the southern parts of the Ridge during the austral winter, but the strong winds do not reach Walters Shoal.

SST showed strong gradients along the ridge between 26 and 40°S, ranging between 6 and 9°C throughout the year. This means that SST at Walters Shoal ranges from 19°C in August to 24°C in February, and at MAD-Ridge from 23°C in August to 27°C in February, in each case a 4–5°C difference. By comparison, SSTs at La Pérouse range from 25 to 28°C, a 1–2°C difference from the situation at MAD-Ridge. The small difference is clearly helped by the south-flowing warm water of the S-EMC, which passes La Pérouse in the form of the South Equatorial Current, as seen by the configuration of the 23°C isotherm in Fig. 3c and d.

MLD is uniform throughout the entire region in summer at ~40 m, but deepens over the northern ridge (at MAD-Ridge) in winter to ~60 m and then to ~100 m at Walters Shoal and La Pérouse. These climatological mean depths do not correspond with cruise CTD data collected in November 2009 (summer) by Read and Pollard (2017), who using temperature and salinity vertical profiles for the Sapmer seamount at similar latitude (37°S, 52°E) but to the east on the SWIR, observed the MLD around 130 m, but with large variance between 70 and 180 m on time-scales of 24 h as a consequence of internal tides. Comparison with Pollard and Read, 2017 revealed the Sapmer seamount to be in the centre of an intense (SSH ~140 cm) anticyclonic eddy, which deepens the thermocline (Dufois et al., 2016). This eddy probably was spun-off the ARC. Given the eddy field over the Madagascar Ridge, large actual MLD variance should be expected.

EKE is the energy associated with the turbulent part of fluid flow, and notably highlights areas/regions with abundant mesoscale eddies. Apart from redistributing momentum and physical tracers, mesoscale eddies, through their lateral stirring, mixing and vertical advection of nutrients, substantially influence phytoplankton distributions, biogeochemical cycles and pelagic ocean ecosystems (e.g. McGillicuddy et al., 1998; Garçon et al., 2001; Yoder et al., 2010; Chelton et al., 2011a, b). Depending on their SSH, they invoke strong rotational currents, as seen in Fig. 6 of our analysis. Our results for EKE revealed the northern part of the Ridge to be highly energetic in eddy activity, with the MAD-Ridge seamount being on the southern edge of a high EKE corridor. A small seasonal signal was detected in the corridor, with greater EKE between March and August. For the three seamounts, EKE was therefore highest at MAD-Ridge (850 cm<sup>2</sup> s<sup>-2</sup> in winter), followed by La Pérouse (185 cm<sup>2</sup>

 $\rm s^{-2}$  in summer), then Walters Shoal (56 cm²  $\rm s^{-2}$ ). The eddy field drives the current field, so speeds will similarly follow this trend (discussed further below).

Anticyclonic subtropical gyres in the oceans are regions of permanent downwelling and consequently deep nutriclines, which limits algal development and subsequent biological and biogeochemical processes (Tomczak and Godfrey, 1994). Morel et al. (2010), using satellite-derived annual means over 10 years (1998–2007) showed chl-a concentrations for the South Indian gyre to be 0.049 ( $\pm$ 0.006) mg m<sup>-3</sup>, with a small but significant season cycle. Lowest values were in December and highest values in August, two months after the winter solstice. Low nutrient availability in the (sub)tropical oligotrophic ocean causes a dominance of cyanobacteria such as Synechococcus and Prochlorococcus over picoeukaryotic phytoplankton species (Li, 1994; Johnson et al., 2006). The domain of this study resides on the western edge of the South Indian subtropical gyre (see Morel et al., 2010; their Fig. 1), so we would expect chl-a mean values in our study to be a little higher than those given in results for the gyre centre. Our chl-a maps in Fig. 3i and j concur with this and similarly highlight the oligotrophic nature of the region, with summer concentrations uniformly  $\sim 0.1$  mg m<sup>-3</sup> over the domain. However, this situation changes in winter, with the area east of the Madagascar Ridge remaining low in chl-a (0.12 mg  $m^{-3}$ ) and that west of the ridge approaching 0.3 mg  $m^{-3}$ . The longitudinal divide is aligned with the eastward base of the ridge, implying that Walters Shoal is located in the elevated chl-a zone. This situation is shown in Table 2, with a climatological mean of  $0.26~\text{mg m}^{-3}$ . MAD-Ridge, on the other hand, with a winter value of 0.19 mg m<sup>-3</sup>, is positioned right on the climatological divide. Seasonal mean chl-a concentrations at La Pérouse remained particularly low at 0.07 mg m<sup>-3</sup> in summer and 0.12 mg m<sup>-3</sup> in winter, confirming its location at the periphery of the gyre. Demarcq et al. (2020) took this analysis further, and using a unique analysis based on a satellite-derived chl-a enrichment index (EI) for the same domain, showed local enrichment at Walters Shoal and at the nearby deeper WS-2 seamount (480 m from the surface). La Pérouse and MAD-Ridge in their analysis exhibited sporadic or no measurable surface chl-a maxima. However, it must be stressed that both this work and that of Demarcq et al. (2020) are climatological analyses and eliminate chl-a signals generated by the shorter time-scales of mesoscale dynamics, as mentioned by Vianello et al. (2020).

# 4.2. Circulation (connectivity)

As pointed out already, much is known about the boundary currents in the South West Indian Ocean: the AC (Agulhas Current), the EMC (East Madagascar Current), and to a lesser extent the ARC (Agulhas Return Current). These have attracted international attention owing to their important role in the global thermohaline circulation (Rahmstorf, 2003). In determining the characteristics, and particularly the volume transport, expensive projects have deployed moorings across the Mozambique Channel (Ridderinkhof and de Ruijter, 2003), the AC (Beal and Bryden, 1999; Morris et al., 2017) and more recently the EMC

(Nauw et al., 2008). The bottom of the S-EMC has also received attention, because it is one of the tributaries of the AC. Those studies highlighted the dynamic nature of the region, with varying endpoint configurations including retroflection (Lutjeharms, 1988) and the generation of dipole eddies (de Ruijter et al., 2004). Owing to the remoteness of the South Indian Ocean, studies on the ARC have relied on remote sensing, in particular satellite-derived altimetry (Read and Pollard, 1993; Lutjeharms and Ansorge, 2001; Quartly and Srokosz, 2003).

In contrast, little is known of the central region of the SWIO, which includes the central and southern parts of the Madagascar Ridge. Read and Pollard (2017), for the only other seamount study in the SWIO, used AVISO altimetry data to demonstrate that the area shows slow mean westward flow between the southern tip of Madagascar and the ARC. Integrated into this are slow (4.1 cm s $^{-1}$ ), west-propagating eddies. These control the currents at each of the five seamounts on the SWIR and one on the Madagascar Ridge, a deep seamount called Walter (1250 m), slightly northeast of Walters Shoal. The latter tended to experience eddies coming from the northeast, producing currents with a mean speed of 18 cm s $^{-1}$  and a maximum of 27 cm s $^{-1}$  (3-year time-series).

In the absence of in situ data, we too used satellite-derived altimetry data to estimate the geostrophic current field in this SWIO. Our velocity vector maps highlighted the main peripheral currents, the AC, the EMC and the ARC, with no obvious seasonal changes at this level of investigation. And as with Read and Pollard (2017), they confirmed the central region of the SWIO, including the central and southern parts of the Madagascar Ridge, as having low current speeds. However, the use of virtual moorings based on 4-day altimetry data along the Madagascar Ridge revealed far more detail of the circulation over the Ridge. As highlighted in Fig. 6, the evolution of currents over the ridge is seen with the passing of eddies. Our analysis showed a strong gradient in current speed along the ridge, with strong (mean 58 cm s<sup>-1</sup>; max. 118 cm s<sup>-1</sup>) unidirectional flow at the northern extreme, and much slower, highly variable flow (mean 8.8 cm s<sup>-1</sup>; max. 24.5 cm s<sup>-1</sup>) near Walters Shoal. At the very southern reaches of the ridge, currents strengthen a little. Those current regimes (gradients) are clear in Fig. 8.

The implications of these results relate to connectivity in terms of the dispersion of biota (larvae). In particular, we estimate that dispersion from MAD-Ridge, which is located between the dominant southwesterly flow of the S-EMC and the eastward flow of the SICC, will be mostly zonal, with greater weight likely to eastward advection. Likewise, dispersion from Walters Shoal, which has low velocity and a highly variable current regime, is likely to be omnidirectional and, relative to MAD-Ridge, restricted in distance. We did not undertake a full-depth analysis for La Pérouse, but given the low EKE (179 cm<sup>2</sup> s<sup>-2</sup>), indicative of moderate eddy intensity and frequency (and hence variable current direction), and its position in the South Equatorial Current (SEC), with a mean velocity  $\sim 19$  cm s<sup>-1</sup>, dispersion is likely to be omnidirectional but distance-restricted, but with an overall westward movement towards Madagascar. Confidence in these extrapolations is provided by the comparison of our geostrophic currents with actual in situ surface drift buoys (see Supplementary Fig. S2). Indeed, these extrapolations are confirmed in Crochelet et al. (2020), who used an individually based model (IBM) to investigate the connectivity of seamounts in the SWIO. That model was driven by OSCAR data.

# 5. Conclusions

This study aimed to provide a SWIO regional view of surface wind as a driver (upwelling and mixing), SST, MLD and chl-*a* as key water column properties, and EKE and currents as drivers of seamount processes and dispersion/connectivity. We used satellite-derived mean seasonal climatologies for these parameters with data spanning 16–22 years. EKE and current speeds were high in the regional boundary currents (i.e. AC, S-EMC and ARC), but low over the central parts of the region, notably the southern part of the Madagascar Ridge. Neither EKE nor velocities

show much seasonality. The strongest longitudinal gradients across the region in winter were for wind, SST, MLD and  ${\rm chl}$ -a.

We had particular focus on characterising the upper ocean environment near the three prominent shallow seamounts, Walters Shoal, MAD-Ridge and La Pérouse. To this end, we showed, relative to the other two seamounts, Walters Shoal to have the lowest mean wind speed (6.7 m s $^{-1}$  in winter), the lowest mean SST (18.4  $^{\circ}\text{C}$  in winter), a deep mean MLD (82 m in winter), the lowest mean current speed (10.7 cm s $^{-1}$ ) and the highest mean chl-a (0.26 mg m $^{-3}$  in winter). It also had the lowest mean EKE (53 cm $^2$  s $^{-2}$ ), indicative of low intensity, less frequent eddies, so dispersion away from it would be limited.

La Pérouse, situated in the trade winds ( $\sim$ 8 m s $^{-1}$ ), has the highest mean SST (27.7 °C in summer), surprisingly the deepest mean MLD (84 m during winter) and intermediate mean current speeds ( $\sim$ 19 cm s $^{-1}$ ). Mean chl-a levels were the lowest (0.07 mg m $^{-3}$ ) there, relative to the other seamounts. Mean EKE (179 cm $^2$  s $^{-2}$ ) was almost four times that at Walters Shoal. Dispersion from La Pérouse will therefore be greater than from Walters Shoal, but still limited.

MAD-Ridge in contrast is located in a much more energetic environment, with faster currents (mean  ${\sim}42~\rm cm~s^{-1}$ ), frequently passing eddies (high mean EKE of  ${\sim}850~\rm cm^2~s^{-2}$ ) and high SSTs (mean 25.8  $^{\circ}C$  in summer) for its latitude, owing to the southward transport of tropical warm water by the S-EMC. Dispersion and connectivity are therefore expected to be greatest for MAD-Ridge.

The results given here provide, in our opinion, an appropriate backdrop for the detailed, ship-based, physical and biological studies presented elsewhere in the MAD-Ridge special issue, underpinning the enhanced knowledge gained on the pelagic ecosystems in the vicinity of these shallow seamounts.

## Declaration of competing interest

We wish to confirm that there are no known conflicts of interest.

# Acknowledgements

The work was supported financially and logistically by the Institut de Recherche pour le Développement (IRD) and the Flotte Océanographique Française. Additional funding was received from the Fonds Français pour l'Environnement Mondial (FFEM) on the Areas Beyond National Jurisdiction (ABNJ) in the South West Indian Ocean. The MADRidge Project was a joint venture between the IRD (France), UBO (Université de Bretagne Occidentale) and the Nelson Mandela University (NMU) in South Africa, with support from the Newton Fund and National Research Foundation (NRF) in the form of the UK-SA Bilateral Research Chair in Ocean Science and Marine Food Security. The MADRidge Project was carried out under the auspices of the Western Indian Ocean Upwelling Research Initiative (WIOURI), which is part of the 2016–2025 International Indian Ocean Expedition (IIOE-2) programme (Roberts, 2015).

#### Appendix A. Supplementary data

Supplementary data to this article can be found online at https://doi.org/10.1016/j.dsr2.2020.104816.

# References

Atlas, R., Hoffman, R., Ardizzone, J., Leidner, S., Jusem, J., Smith, D., Gombos, D., 2011.
A cross-calibrated, multiplatform ocean surface wind velocity product for meteorological and oceanographic applications. Bull. Am. Meteorol. Soc. 92, 157-174

Beal, L., Bryden, H., 1999. The velocity and vorticity structure of the Agulhas Current at  $32^\circ$  S. J. Geophys. Res. Oceans 104 (C3), 5151–5176.

Braby, L., Backeberg, B., Ansorge, I., Roberts, M., Krug, M., Reason, C., 2016. Observed eddy dissipation in the Agulhas current. Geophys. Res. Lett. 43 (15), 8143–8150.

- Chelton, P.B., Gaube, P., Schlax, M.G., Early, J.J., Samelson, R.M., 2011b. The influence of nonlinear mesoscale eddies on near-surface oceanic chlorophyll. Science 334 (6054), 328–332. https://doi.org/10.1126/science.1208897.
- Chelton, D.G., Schlax, M.G., Samelson, R.M., 2011a. Global observations of nonlinear mesoscale eddies. Prog. Oceanogr. 91 (2), 167–216.
- Clark, M.R., Vinnichenko, V.I., Gordon, J.D.M., Beck-Bulat, G.Z., Kukharev, N.N., Kakora, A.F., 2007. Large-scale distant-water trawl fisheries on seamounts. In: Pitcher, T.J., Morato, T., Hart, P.J.B., Clark, M.R., Haggan, N., Santos, R.S. (Eds.), Seamounts: Ecology, Fisheries and Conservation 12. Blackwell Publishing, Oxford, U.K, pp. 361–399.
- Clark, M.R., Schlacher, T.A., Rowden, A.A., Stocks, K.I., Consalvey, M., 2012. Science priorities for seamounts: research links to conservation and management. PloS One 7 (1), e29232. https://doi.org/10.1371/journal.pone.0029232.
- Collins, M., Roberts, M.J., Ternon, J-F., Demarcq, H., Herbette, S., in preparation. Event-scale (3–10 Days) Observations of Upwelling on the Southeast Coast of Madagascar.
- Crochelet, E., Barrier, N., Andrello, M., Marsac, F., Spadone, A., Lett, C., 2020.

  Connectivity between seamounts and coastal ecosystems in the Southwestern Indian Ocean. Deep-Sea Res. II (this issue).
- de Boyer Montégut, C., Madec, G., Fischer, A., Lazar, A.S., Iudicone, D., 2004. Mixed layer depth over the global ocean: an examination of profile data and a profile-based climatology. J. Geophys. Res. 109 (C12) https://doi.org/10.1029/2004JC002378.
- Demarcq, H., Noyon, M., Roberts, M.J., 2020. Satellite observations of phytoplankton enrichments around seamounts in the South West Indian Ocean, with a special focus on the Walters Shoal. Deep-Sea Res. II (this issue).
- de Ruijter, W., van Aken, H., Beier, E., Lutjejarms, J.R.E., Matano, R., Schouten, W., 2004. Eddies and dipoles around South Madagascar: formation, pathways and largescale impact. Deep-Sea Res. I 51, 383–400.
- Dilmahamod, A.F., Penven, P., Aguiar-González, B., Reason, C.J.C., Hermes, J.C., 2019.
  A new definition of the South-East Madagascar bloom and analysis of its variability.
  J. Geophys. Res. Oceans 124. https://doi.org/10.1029/2018JC014582.
- Dufois, F., Hardman-Mountford, N., Greenwood, J., Richardson, A., Feng, M., Matear, R., et al., 2016. Anticyclonic eddies are more productive than cyclonic eddies in subtropical gyres because of winter mixing. Science Advances 2 (5), e1600282. https://doi.org/10.1126/sciadv.1600282.
- Evano, H., Bourjea, J., 2012. Atlas de la pêche palangrière réunionnaise de l'océan Indien. RST 245 doi/2012-11.
- Garçon, V., Oschlies, A., Doney, S., McGillicuddy, D., Waniek, J., 2001. The role of mesoscale variability on plankton dynamics in the North Atlantic. Deep-Sea Res. II 48, 2199–2226.
- Goslin, J., Segoufin, J., Schlich, R., Fisher, R.L., 1980. Submarine topography and shallow structure of the Madagascar Ridge, western Indian Ocean. GSA Bull. 91 (12), 741–753.
- Halo, I., Penven, P., Backeberg, B., Ansorge, I., Shillington, F., Roman, R., 2014. Mesoscale eddy variability in the southern extension of the East Madagascar Current: seasonal cycle, energy conversion terms, and eddy mean properties. J. Geophys. Res. Oceans 119 (10), 7324–7356.
- Harris, P.T., MacMillan-Lawler, M., Rupp, J., Baker, E.K., 2014. Geomorphology of the oceans. Mar. Geol. 352, 4–24.
- Harris, S.A., Noyon, M., Marsac, F., Vianello, P., Roberts, M.J., 2020. Ichthyoplankton assemblages at three shallow seamounts in the South West Indian Ocean. Deep-Sea Res. II (this issue).
- Johnson, Z.I., Zinser, E.R., Coe, A., McNulty, N.P., Woodward, E.M.S., Chisholm, S.W., 2006. Niche partitioning among *Prochlorococcus* ecotypes along ocean-scale environmental gradients. Science 311, 1737–1740.
- Seamounts, islands and atolls. In: Keating, B.H., Fryer, P., Batiza, R., Boehlert, G.W. (Eds.), Geophys. Monogr. 43, 319–334.
- Kitchingman, A., Lai, S., Morato, T., Pauly, D., 2007. How many seamounts are there and where are they located? In: Pitcher, T., Morato, T., Hart, P., Clark, M., Haggan, N., Santos, R. (Eds.), Seamounts: Ecology, Fisheries and Conservation. Fisheries and Aquatic Resources Series. Blackwell, Oxford, pp. 26–40.
- Lavelle, J., Mohn, C., 2010. Motion, commotion, and biophysical connections at deep ocean seamounts. Oceanography 23, 90–103.
- Li, W.K.W., 1994. Primary production of prochlorophytes, cyanobacteria, and eukaryotic ultraphytoplankton measurements from flowcytometric sorting. Limnol. Oceanogr. 39, 169–175
- Littler, M.M., Littler, D.S., Blair, S.M., Norris, J.N., 1986. Deep-water plant communities from an uncharted seamount off San Salvador Island, Bahamas: distribution, abundance, and primary productivity. Deep-Sea Res. I 33, 881–892.
- Lutjeharms, J.R.E., 1988. Remote sensing corroboration of retroflection of the East Madagascar Current. Deep-Sea Res. A 35, 2045–2050.
- Lutjeharms, J.R.E., 2006. The Agulhas Current. Springer, New York, p. 334.
- Lutjeharms, J.R.E., 2007. Three decades of research on the greater Agulhas Current. O. Sci. Europ. Geosci. Un. 3 (1), 129–147.
- Lutjeharms, J.R.E., Ansorge, I., 2001. The Agulhas Return current. J. Mar. Syst. 30, 115–138.
- McGillicuddy, D.J., Robinson, A.R., Siegel, D.A., Jannasch, H.W., Johnson, R., Dicky, T. D., McNeil, J., Michaels, A.F., Knap, A.H., 1998. Influence of mesoscale eddies on new production in the Sargasso Sea. Nature 394, 263–266.
- Morel, A., Claustre, H., Gentilli, B., 2010. The most oligotrophic subtropical zone of the global ocean: similarities and difference in terms of chlorophyll and yellow substance. Biogeosciences 7, 3139–3151.

- Morris, T., Hermes, J., Beal, L., du Plessis, M., Duncombe-Rae, C., Gulekana, M., Lamont, T., Speich, S., Roberts, M., Ansorge, I.J., 2017. The importance of monitoring the Greater Agulhas Current and its inter-ocean exchanges using large mooring arrays. South Afr. J. Sci. 113 (7/8) https://doi.org/10.17159/sajs.2017/20160330
- Nauw, J.J., van Aken, H.M., Webb, A., Lutjeharms, J.R.E., de Ruijter, W.P.M., 2008. Observations of the southern East Madagascar Current and undercurrent and counter current system. J. Geophys. Res. 113, C08006. https://doi.org/10.1029/ 2007JC004639.
- Palastanga, V., van Leeuwen, P.J., Schouten, M.W., de Ruijter, W.P.M., 2007. Flow structure and variability in the subtropical Indian ocean: instability of The south Indian Ocean Countercurrent. J. Geophys. Res. Oceans 112 (C1). https://doi.org/ 10.1029/2005JC003395.
- Parin, N.V., Mironov, A.N., Nesis, K.N., 1997. Biology of the Nazca and Sala y Gomez submarine ridges, an outpost of the Indo-West Pacific fauna in the eastern Pacific Ocean: composition and distribution of the fauna, its communities and history. Adv. Mar. Biol. 32, 145–242.
- Pinet, P., Jaquemet, S., Phillips, R.A., Le Corre, M., 2012. Sex-specific foraging strategies throughout the breeding season in a tropical, sexually monomorphic small petrel. Anim. Behav. 83, 979–989. https://doi.org/10.1012/j.anbehav.2012.01.19.
- Pollard, R., Read, J., 2017. Circulation, stratification and seamounts in the south west Indian Ocean. Deep-Sea Res. II 136, 36–43. https://doi.org/10.1016/j. dsr2.2015.02.018.
- Quartly, G., Buck, J., Srokosz, M., Coward, C., 2006. Eddies around Madagascar the retroflection re-considered. J. Mar. Syst. 63 (3–4), 115–129.
- Quartly, G.D., Srokosz, M.A., 2003. Satellite observations of the Agulhas current system. Phil. Trans. Appl. Math. Phys. Eng. Sci. 361, 51–56. https://doi.org/10.1098/rsta.2002.1107, 1802.
- Rahmstorf, S., 2003. The current climate. Nature 421, 699.
- Read, J., Pollard, R., 1993. Structure and transport of the Antarctic circumpolar current and Agulhas Return current at 40°E. J. Geophys. Res. Oceans 98 (C7), 12281–12295.
- Read, J., Pollard, R., 2017. An introduction to the physical oceanography of six seamounts in the southwest Indian Ocean. Deep Sea Res. II 136, 44–58.
- Richer de Forges, B., Koslow, J., Poore, G., 2000. Diversity and endemism of the benthic seamount fauna in the southwest Pacific. Nature 405, 944–947.
- Ridderinkhof, H., de Ruijter, W.P.M., 2003. Moored current observations in the Mozambique Channel. Deep-Sea Res. II 50, 1933–1955.
- Ridderinkhof, W., Le Bars, D., von der Heydt, A.S., de Ruijter, W.P.M., 2013. Dipoles of the south east Madagascar current. Geophys. Res. Lett. 40 (3), 558–562.
- Roberts, M., 2015. The western Indian Ocean Upwelling research initiative (WIOURI): a flagship IIOE2 project. No. 68 CLIVAR Exch. 19 (3). Nov 2015.
- Roberts, M., Ternon, J.-F., Morris, T., 2014. Interaction of dipole eddies with the western slope of the Mozambique Channel. Deep-Sea Res. II 100, 54–67. https://doi.org/10.1016/j.dsr2.2013.10.016.
- Roberts, M.J., Ternon, J.-F., Marsac, F., Noyon, M., Payne, A.I.L., 2020. The MADRidge Project: bio-Physical coupling around three shallow seamounts in the South West Indian Ocean. Deep-Sea Res. II (this issue).
- Rogers, A.D., 1994. The biology of seamounts. Adv. Mar. Biol. 30, 305–350.
- Rogers, A.D., Alvheim, O., Bemanaja, E., Benivary, D., Boersch-Supan, P., Bornman, T.G., Cedras, R., Du Plessis, N., Gotheil, S., Høines, A., Kemp, K., Kristiansen, J., Letessier, T., Mangar, V., Mazungula, N., Mørk, T., Pinet, P., Pollard, R., Read, J., Sonnekus, T., 2017. Pelagic communities of The South West Indian ocean seamounts: R/V Dr Fridijof ansen cruise 2009–410. Deep-Sea Res. II 136, 5–35.
- Rubin, M.J., van Loon, H., 1953. Aspects of the circulation of the southern hemisphere. J. Meteorol. 11, 68–76.
- Siedler, G., Rouault, M., Biastoch, A., Backeberg, B., Reason, C.J.C., Lutjeharms, J.R.E., 2009. Modes of the southern extension of the east Madagascar current. J. Geophys. Res. 114 https://doi.org/10.1029/2008JC004921. C01005.
- Siedler, G., Rouault, M., Lutjeharms, J.R.E., 2006. Structure and origin of the subtropical south Indian Ocean Countercurrent. Geophys. Res. Lett. 33 (24) https://doi.org/ 10.1029/2006GL027399.
- Srokosz, M.A., Robinson, J., McGrain, H., Popova, E.E., Yool, A., 2015. Could the Madagascar bloom be fertilized by Madagascan iron? J. Geophys. Res. Oceans 120, 5790–5803. https://doi.org/10.1002/2015JC011075.
- Stramma, L., Lutjeharms, J.R.E., 1997. The flow field of the subtropical gyre of the South Indian Ocean. J. Geophys. Res. 102 (C3), 5513–5530.
- Thistle, D., 2003. The deep-seafloor: an overview. In: Tyler, P.A. (Ed.), Ecosystems of the World 28, Ecosystems of the Deep Oceans, Chapter 2. Elsevier Science, Amsterdam. Tomczak, M., Godfrey, J.S., 1994. Regional Oceanography: an Introduction, Percamon.
- Tomczak, M., Godfrey, J.S., 1994. Regional Oceanography: an Introduction. Pergamon Press, Oxford, ISBN 008-0410200, p. 422.
- Tyler, P., Bronsdon, S., Young, C., Rice, A., 1995. Ecology and gametogenic biology of the genus *umbellula* (pennatulacea) in the north atlantic. Int. Rev. Gesamten Hydrobiol. Hydrogr. 80, 187–199.
- Vianello, P., Herbette, S., Ternon, J.-F., Demarcq, H., Roberts, M.J., 2020. Observation of a mesoscale eddy dipole on the northern Madagascar Ridge: consequences for the circulation and hydrography in the vicinity of a seamount. Deep-Sea Res. II (this issue).
- Yoder, J., Doney, S., Siegel, D., Wilson, C., 2010. Study of marine ecosystems and biogeochemistry now and in the future: examples of the unique contributions from space. Oceanography 23 (4), 104–117. Retrieved 6 June 2020, from. www.jstor. org/stable/24860866.